Supporting Information

Kobayashi et al. 10.1073/pnas.1800294115

SI Materials and Methods

Refrigeration and Magnetic Exposure System. As shown in Fig. S1, we modified the experimental freezing chamber for water-filled balloons described by Kobayashi et al. (1) to have a slightly larger Styrofoam box capable of housing a three-axis set of square Helmholtz coils, designed to nest within each other (Fig. 1*A* of the main text), within a temperature-controlled environment. The coils were constructed from 2-cm plastic U-channels with outside diameters of 32, 28, and 24 cm, respectively for the two horizontal axes (x, y) and the vertical axis (z), respectively. Each coil contained 300 total turns (150 × 2) of #20-gauge copper magnet wire, and the coil pairs were spaced at the square Helmholtz criterion for uniform central fields which has a separation of 0.545 of the coil edge length [compared with 0.5 diameter separations for the standard circular Helmholtz case; see table 1A of Kirschvink (2)]. A computer-driven circuit controls the settings of the three DPDT relays (one for each axis), which are configured to invert the direction of current flowing in one winding in each set of coils, toggling between the active and active-sham conditions shown in Fig. 1 *B* and *C*. The horizontal x and y axes are configured to produce a constant-strength rotating magnetic field vector at the center, using an Owon AG1022F dual-channel digital function generator to produce both a 10-Hz sine-wave and a 90° shifted (cosine-wave) output. These outputs are fed into left and right channels of a Crest model 8200 audio amplifier, and the amplitudes are configured to produce the desired field strength for the horizontally rotating vector. A DC power supply is used to produce a constant amplitude, downward-directed vertical component (z axis). Calibration was done using a FW Bell 5180 digital Hall-probe gaussmeter. Measured coil heating was minimal for field strengths below ∼2 mT; hence, we chose to do our experiments at 0-, 0.5-, 1.0-, and 1.5-mT levels.

Nanophase Magnetite. For these experiments, we used nanophase, aqueously precipitated magnetite obtained from Toda Kogyu Corporation in a stabilized liquid emulsion of particles with a nominal particle size of 50 nm; particles prepared by aqueous precipitation have fewer clumping problems than emulsions prepared from powders. These particles are single magnetic domains that are stably and uniformly magnetized at the saturation value, J_s, of 4.8×10^5 A/m (∼92 Am^2/kg). Images of these particles were taken on a JEM-1400plus transmission electron microscope at 100 kV and generally confirm the manufacturer' specification of the crystals.

Water, Balloons, and Freezing Volume Change. As in our previous study (1), we used ultrapure water samples from a Yamato Scientific Company WA203 ion exchange/distillation unit. As even the best of these water distillation and purification units can leave parts-per-billion levels of ferromagnetic nanoparticles suspended the water [which are commonly leached from laboratory plastics and glassware (3)], we placed strong NdFeB magnets near the bottom of the water storage vessel for several days, allowing the strong field gradients to gradually sequester the magnetic particles. Water samples for our studies were decanted from the top when needed. As ferric iron minerals are soluble at low pH, all containers were washed in concentrated HCl before use to solve the contamination problem (3). We then made standard balloons out of stretchable, ∼0.1-mm-thick, acid-washed Thermoplastic PolyUrethane film (TG88-I tough grace film; Takeda Sangyo Company), which were filled with ∼150 g of water, without air bubbles, using an acid-washed glass syringe. These balloons were suspended at the center of the Helmholtz coil system in a plastic framework, with digital thermocouples taped to the top and bottom for taking readings at 1-s intervals, as before (1). Comparisons reported below were made with the ultrapure water that had been spiked with the well-characterized magnetite nanocrystals mentioned above. To monitor actual volume change of the water before and after freezing, we used the chilled ethanol immersion technique described previously (1). All experimental field and frequency conditions were run with groups exposed to the actual magnetic field condition, and associated ones in which the active-sham condition was used.

Data Quantification and Statistical Analysis. These experiments were similar in design to those of Kobayashi et al. (1). Except for the application of rotating magnetic fields of various strengths, we used the same quantification and statistical analysis methods as in that previous study. In this study, we ran between six and nine trials at each magnetic field condition, each of active magnetic field, and the active sham, as shown in Tables S1–S4. The quantitative measure of volume change was computed as a percentage, taken directly from before and after freezing as mentioned above. For the measure of supercooling, we used the lowest temperature reached before the abrupt spike to the melting point (∼0 °C) that results from the release of the latent heat of freezing (∼80 cal/g for water). Following the recommendation of Saville (4), the null hypothesis of no effect is tested easily with Student's t test of means for unpaired samples with unequal variance (heteroscedastic), using two-tailed tests. The independence of the volumetric and thermal analyses, and the overall simplicity, argues that a more complex ANOVA is not needed (4).

Rock Magnetic Experiments to Determine Particle Concentration and Size. Superconducting moment magnetometry using SQUID sensors has the ability to detect subpicogram levels of ferromagnetic materials dispersed in ∼10-g samples (5–8). We measured the concentrations of magnetite in our spiked water samples using a 2G Enterprises model 760, three-axis vertical superconducting rock magnetometer (SRM) housed in a class-1000 magnetically shielded clean laboratory at Caltech. The sample access chamber of the magnetometer was held at ∼−20 °C by running a small flow of dry nitrogen gas through a HEPA filter, then through a coiled copper tube immersed in a Dewar of liquid nitrogen, and then into the bottom end of the SRM. Temperature was monitored using nonmagnetic fiber optic thermal sensing system from Omega for which the fiber sensors had been run through the vertical sense region of the magnetometer. Water samples (ultrapure and magnetite-spiked) were frozen in acid-washed quartz-glass cups while sitting on a chilled aluminum plate assembly as described previously (1). Cylindrical ice samples produced in this fashion were removed from the quartz holders by gently warming the glass, and suspended from the vertical sample system of the SRM on ∼15-cm-long, thin, acid-washed monofilament lines frozen into the center of the ice. The ice samples were exposed to a brief (∼1-ms) vertical magnetic pulse of 0.8 T to impart an isothermal remanent magnetization along the vertical axis, and the moment so acquired was measured using the vertical SQUID sensor of the SRM. Representative data are shown in Table S5.

Supercooling of Representative Plant and Animal Tissues. As various animal and plant tissues are known to contain trace amounts of nanophase magnetite (5, 9), we chose to test the magnetic inhibition

of freezing on one sample of each. Celery stocks (*Apium graveolens*, var. *dulce*) were obtained from local growers, and a fresh sample of bovine muscle tissue (*Bos taurus*, var. *kuroge wagyu*) was obtained from a local butcher in Tokyo as a freshly cut chunk. Once in the laboratory, all samples were handled using plastic tools and glass or plastic surfaces washed in concentrated HCl and cleaned in the purified water described above. They were then subsampled onto ~50-g cubes using acid-washed ceramic knives and wrapped tightly in washed, EM-grade Mylar film. Mylar film was also used to fasten tightly a pair of thin wire thermocouples to the top and bottom surface of the samples, similar to that of the water balloon samples. These were also positioned in the center of the coil system for the freezing experiments, with data recorded in the same manner.

1. Kobayashi A, Golash HN, Kirschvink JL (2016) A first test of the hypothesis of biogenic magnetite-based heterogeneous ice-crystal nucleation in cryopreservation. *Cryobiology* 72:216–224.
2. Kirschvink JL (1992) Uniform magnetic fields and double-wrapped coil systems: Improved techniques for the design of bioelectromagnetic experiments. *Bioelectromagnetics* 13:401–411.
3. Kobayashi AK, Kirschvink JL, Nesson MH (1995) Ferromagnetism and EMFs. *Nature* 374:123.
4. Saville DJ (1990) Multiple comparison procedures–The practical solution. *Am Stat* 44: 174–180.
5. Kirschvink JL, Jones DS, McFadden BJ (1985) *Magnetite Biomineralization and Magnetoreception in Organisms: A New Biomagnetism* (Plenum, New York).
6. Kirschvink JL, Kobayashi-Kirschvink A, Woodford BJ (1992) Magnetite biomineralization in the human brain. *Proc Natl Acad Sci USA* 89:7683–7687.
7. Kobayashi A, et al. (2006) Experimental observation of magnetosome chain collapse in magnetotactic bacteria: Sedimentological, paleomagnetic, and evolutionary implications. *Earth Planet Sci Lett* 245:538–550.
8. Kirschvink JL, Kopp RE, Raub TD, Baumgartner CT, Holt JW (2008) Rapid, precise, and high-sensitivity acquisition of paleomagnetic and rock-magnetic data: Development of a low-noise automatic sample changing system for superconducting rock magnetometers. *Geochem Geophys Geosyst* 9:1–18.
9. Gajdardziska-Josifovska M, McClean RG, Schofield MA, Sommer CV, Kean WF (2001) Discovery of nanocrystalline botanical magnetite. *Eur J Mineral* 13:863–870.

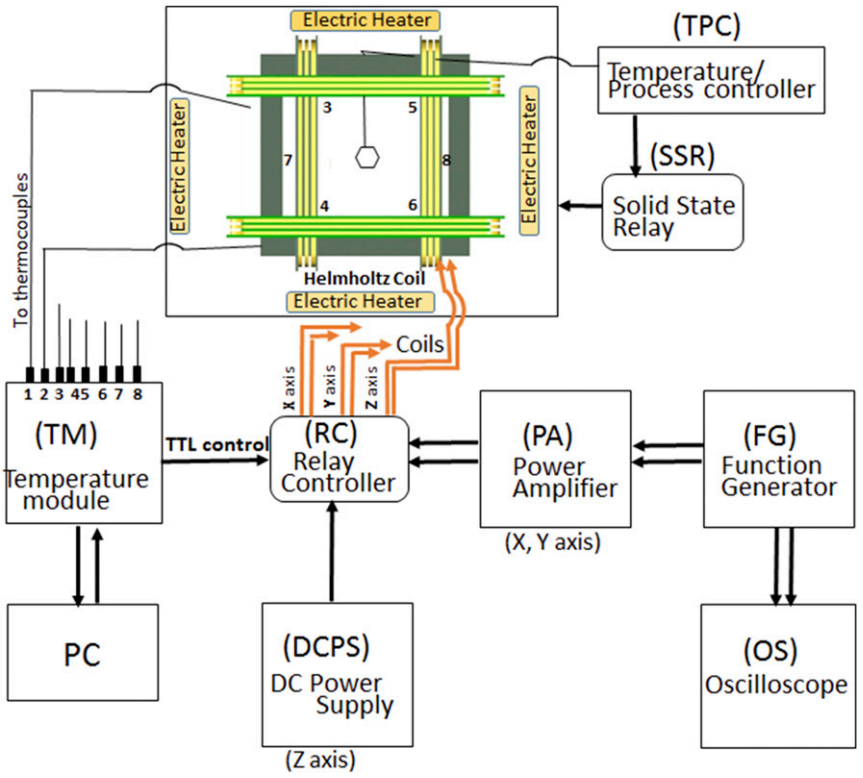

Fig. S1. Components of the experimental setup. Inside a constant −80 °C top-opening freezer (not shown), we suspended a Styrofoam box (o.d., 55-cm length, 46-cm width, and 55-cm high; walls, 2 cm thick) with a removable lid. The inside walls of this box are lined with 0.5-mm copper foil to minimize thermal gradients, and five electric heating pads are positioned along the inside walls and floor of this box. A small electric fan on the top cover (not shown) circulated the air slowly to reduce further thermal gradients. An Omega 76000 temperature process controller (TPC) monitors a thermocouple in the bottom center of the box, and uses a PID tuning protocol and a solid-state relay (SSR) to regulate power to the heaters and maintain the internal environment at a fairly constant temperature of approximately −18 °C. Temperature at eight locations within the experimental chamber (two on the water sample, six others in and around the chamber) were monitored with a measurement computing USB-TC module; these items are similar to those used by Kobayashi et al. (1). The nested set of three square Helmholtz coil pairs (Fig. 1*A*) were supported orthogonally in the middle of the Styrofoam box, and the experimental samples (the water-filled balloon or tissues) held in the center as before (1). Current through the two horizontal axes was programmed with a two-axis function generator (FG) set to produce two 10-Hz sine waves with a phase shift of 90° ($\pi/2$), which were monitored with a dual-beam oscilloscope and fed into a dual-channel audio power amplifier (Crest model #8200) before passing through the coils. The static vertical field was controlled by a 30-V, 5-A (max) DC power supply. Power lines for all three axes were fed through a computer-controlled relay box with double-pole double-throw (DPDT) switches that set the active vs. sham modes for the coils as described on Fig. 1 *A* and *B* in the main text. A digital F. W. Bell Gauss/Tesla meter (Model 5180) was used to calibrate the voltage/field levels for each axis.

1. Kobayashi A, Golash HN, Kirschvink JL (2016) A first test of the hypothesis of biogenic magnetite-based heterogeneous ice-crystal nucleation in cryopreservation. *Cryobiology* 72:216–224.

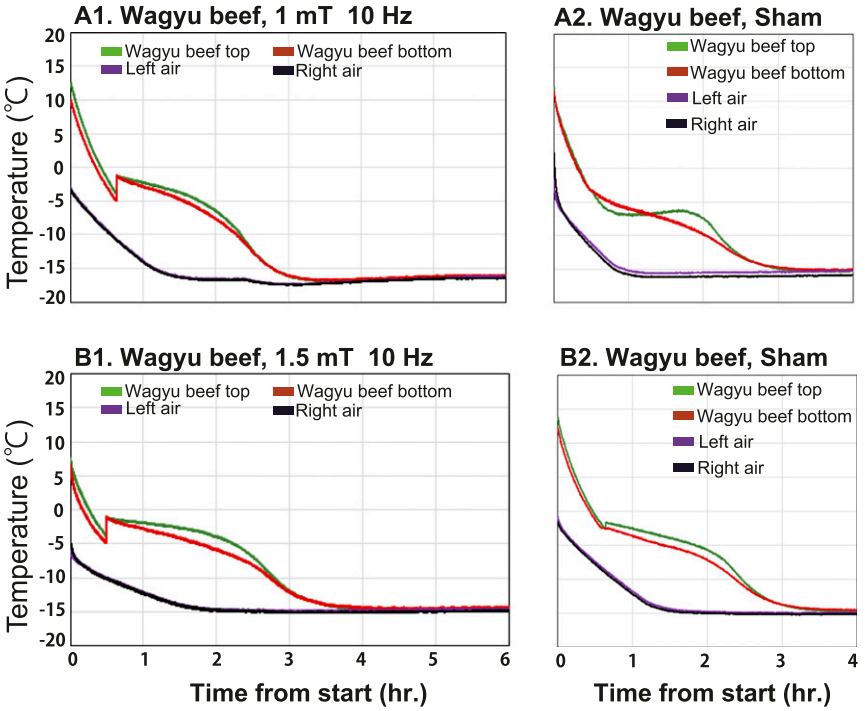

Fig. S2. Preliminary supercooling experiments for ~50-g samples of bovine muscle tissue (*Bos taurus*, var. *kuroge wagyu*), obtained from a local butcher in Meguro, Tokyo. Each experiment was run on a fresh sample of the meat. Although the overall rate of cooling was faster than for the balloons due to the lower sample mass, rotating magnetic fields of 1.0 and 1.5 mT produced clearly visible thermal spikes indicating supercooling. Note that the baseline melting/freezing temperature of the cytoplasm of beef will be slightly lower than 0 °C due to dissolved intracellular ionic materials (salts, peptides, etc.). Left-hand diagrams in each pair (*A1* and *B1*) are from experiments in which the rotating magnetic field was at the strength and intensity indicated. Those in the right-hand column (*A2* and *B2*) are from the sham controls.

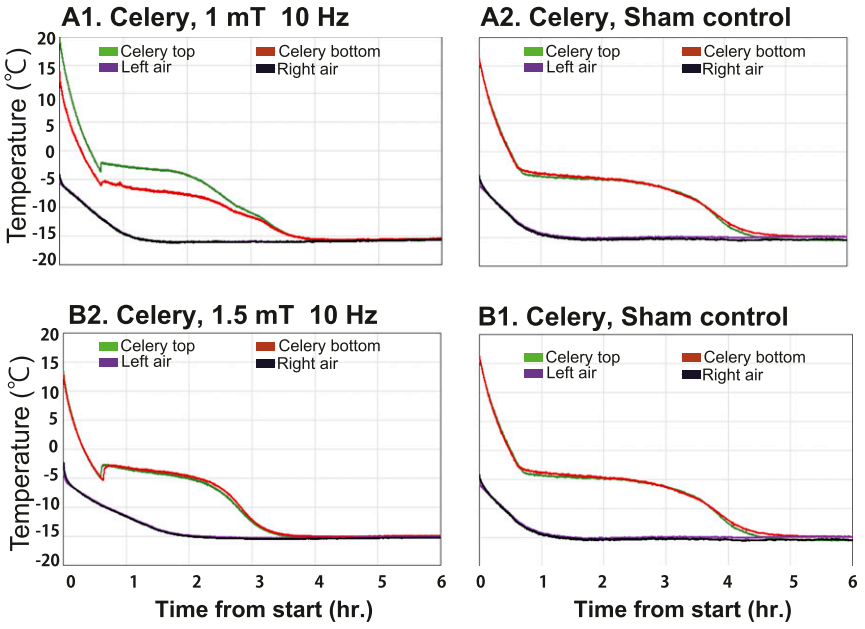

Fig. S3. Preliminary supercooling experiments on samples of celery stocks (*Apium graveolens*, var. *dulce*), obtained from local growers at Hara Village, Nagano Prefecture, Japan. For each of the experiments, two to three segments of the stocks totaling ~50 g were wrapped tightly together inside the EM-grade Mylar film, with fresh (previously unfrozen) to maximize thermal conductivity. Again, the melting/freezing temperature is lower than pure water due to dissolved intracellular ionic materials. Left-hand diagrams in each pair (*A1* and *B1*) are from experiments in which the rotating magnetic field was at the strength and intensity indicated. Those in the right-hand column (*A2* and *B2*) are from the sham controls.

Table S1. Volume and supercooling data for experimental water samples used in these experiments, as well as results from the *t* test of means: Part A

Date of file	Applied field, G	Frequency, Hz	SC temperature (top), °C	Volume before, mL	Volume after, mL	Difference, mL	Volume change, %
A1. Purified water, 1.0 mT, 10 Hz							
04/14/2016	10	10	−9.0	132	141	9	6.8
02/02/2017	10	10	−3.2	162	169	7	4.3
02/08/2017	10	10	−7.1	170	184	14	8.2
02/13/2017	10	10	−9.9	160	175	15	9.3
02/14/2017	10	10	−3.4	148	155	8	5.4
02/15/2017	10	10	−2.4	153	164	11	7.2
	N = 6	Mean T, °C = −5.84				Mean vol% = 6.9	
		SD = 3.25				Std = 1.8	
A2. Purified water, 1.0-mT, 10-Hz sham							
04/12/2016	10 sham	10	−9.7	135	145	10	7.4
04/13/2016	10 sham	10	−11.1	143	155	12	8.4
01/16/2017	10 sham	10	−8.9	167	176	9	5.4
02/09/2017	10 sham	10	−10.8	170	184	14	8.2
02/10/2017	10 sham	10	−6.2	162	176	14	8.6
02/15/2017	10 sham	10	−10.8	160	168	8	5.0
	N = 6	Mean T, °C = −9.59				Mean vol% = 7.2	
		SD = 1.85				Std = 1.6	
		Two-tailed *P* value: 0.040				Two-tailed *P* value: 0.767	

In Tables S1–S4, letters A–D in the boxes correspond to the data groups in Figs. 3 and 4 of the main text. Highly significant differences in both supercooling temperatures and volume were found in the 1.0- and 1.5-mT comparisons between experiments with the field-activated and the corresponding sham conditions.

Table S2. Volume and supercooling data for experimental water samples used in these experiments, as well as results from the *t* test of means: Part B

Date of file	Applied field, G	Frequency, Hz	SC temperature (top), °C	Volume before, mL	Volume after, mL	Difference, mL	Volume change, %
B1. Fe_3O_4 + water, 0.5 mT, 10 Hz							
11/11/2016	5	10	−8.5	162	174	12	7.4
11/15/2016	5	10	−0.4	163	178	15	9.2
11/17/2016	5	10	−7.8	172	187	14	8.1
11/22/2016	5	10	−1.5	167	183	16	9.6
11/26/2016	5	10	−1.9	161	177	16	9.9
11/28/2016	5	10	−2.1	155	170	15	9.7
11/28/2016	5	10	−1.5	160	176	16	10
11/29/2016	5	10	−3.3	171	186	15	9.4
02/16/2017	5	10	−0.4	160	172	12	7.5
	N = 9	Mean T, °C = −3.0				Mean vol% = 9.0	
		SD = 3.0				Std = 1.0	
B2. Fe_3O_4 + water, 0.5-mT, 10-Hz sham							
11/14/2016	5 sham	10	−1.5	162	178	16	9.9
11/24/2016	5 sham	10	−1.6	161	180	19	11.8
11/25/2016	5 sham	10	−3.0	168	186	18	10.1
11/25/2016	5 sham	10	−3.1	149	163	14	9.4
03/08/2017	5 sham	10	−2.0	155	172	17	10.9
03/09/2017	5 sham	10	−0.2	166	182	16	9.6
	N = 6	Mean T, °C = −1.9				Mean vol% = 10.3	
		SD = 1.1				Std = 0.9	
		Two-tailed *P* value: 0.3216				Two-tailed *P* value: 0.0240	

In Tables S1–S4, letters A–D in the boxes correspond to the data groups in Figs. 3 and 4 of the main text. Highly significant differences in both supercooling temperatures and volume were found in the 1.0- and 1.5-mT comparisons between experiments with the field-activated and the corresponding sham conditions.

Table S3. Volume and supercooling data for experimental water samples used in these experiments, as well as results from the *t* test of means: Part C

Date of file	Applied field, G	Frequency, Hz	SC temperature (top), °C	Volume before, mL	Volume after, mL	Difference, mL	Volume change, %
C1. Fe_3O_4 + water, 1.0 mT, 10 Hz							
04/06/2016	10	10	−7.5	175	186	11	6.3
04/07/2016	10	10	−6.9	152	162	10	6.6
04/15/2016	10	10	−5.4	130	143	13	9.1
05/19/2016	10	10	−8.1	170	182	12	5.0
05/24/2016	10	10	−8.3	154	165	11	7.1
05/26/2016	10	10	−8.2	158	167	9	5.7
06/15/2016	10	10	−6.1	156	167	11	7.1
07/13/2016	10	10	−6.6	164	178	14	8.5
	N = 8	Mean T, °C = −7.14				Mean vol% = 6.9	
		SD = 1.07				Std = 1.4	
C2. Fe_3O_4 + water, 1.0-mT, 10-Hz sham							
04/08/2016	10 sham	10	−1.2	137	151	14	10.2
05/20/2016	10 sham	10	−3.1	156	171	15	9.6
12/01/2016	10 sham	10	−1.4	156	174	18	11.5
12/02/2016	10 sham	10	−3.0	170	185	15	9.4
03/03/2017	10 sham	10	−0.1	152	166	14	9.2
03/07/2017	10 sham	10	−2.6	156	172	16	10.3
	N = 6	Mean T, °C = −1.90				Mean vol% = 10.0	
		SD = 1.19				Std = 0.8	
		Two-tailed *P* value: 0.0000061				Two-tailed *P* value: 0.00022	

In Tables S1–S4, letters A–D in the boxes correspond to the data groups in Figs. 3 and 4 of the main text. Highly significant differences in both supercooling temperatures and volume were found in the 1.0- and 1.5-mT comparisons between experiments with the field-activated and the corresponding sham conditions.

Table S4. Volume and supercooling data for experimental water samples used in these experiments, as well as results from the *t* test of means: Part D

Date of file	Applied field, G	Frequency, Hz	SC temperature (top), °C	Volume before, mL	Volume after, mL	Difference, mL	Volume change, %
D1. Fe_3O_4 + water, 1.5 mT, 10 Hz							
06/16/2016	15	10	−9.4	164	169	5	3.48
06/17/2016	15	10	−7.3	171	180	9	5.3
07/25/2016	15	10	−9.2	153	165	12	7.8
09/07/2016	15	10	−9.0	176	188	12	6.8
11/04/2016	15	10	−8.8	158	171	13	8.2
12/02/2016	15	10	−7.8	166	178	12	7.2
	N = 6	Mean T, °C = −8.58				Mean vol% = 6.5	
		SD = 0.84				Std = 1.8	
D2. Fe_3O_4 + water, 1.5-mT, 10-Hz sham							
09/08/2016	15 sham	10	−0.9	152	166	14	9.2
11/08/2016	15 Sham	10	−1.2	162	178	16	9.9
02/22/2017	15 Sham	10	−1.6	154	169	15	9.8
02/24/2017	15 Sham	10	−2.2	156	171	15	9.6
02/28/2017	15 Sham	10	−1.1	170	186	16	9.4
03/02/2017	15 Sham	10	−0.2	164	178	14	8.5
	N = 6	Mean T, °C = −1.2				Mean vol% = 9.4	
		SD = 0.7				Std = 0.5	
		Two-tailed *P* value: 0.00000002				Two-tailed *P* value: 0.00845	

In Tables S1–S4, letters A–D in the boxes correspond to the data groups in Figs. 3 and 4 of the main text. Highly significant differences in both supercooling temperatures and volume were found in the 1.0- and 1.5-mT comparisons between experiments with the field-activated and the corresponding sham conditions.

Table S5. Results of SQUID moment magnetometry for water, magnetite suspended in water, beef, and celery samples

Sample	Mass, g	Saturation remanence, Am^2	Magnetization, Am^2/kg	SD magnetite equivalent, ppb
Purified water	8.0	<8.23E-11	<1.03E-08	<0.04
Fe_3O_4 + water	8.0	1.22E-07	1.52E-05	64.8
Wagyu beef 1	9.1	5.32E-09	5.85E-07	2.5
Wagyu beef 2	7.8	8.32E-09	1.07E-06	4.5
Celery mid 1	7.8	1.05E-09	1.35E-07	0.6
Celery mid 2	7.0	3.34E-09	4.77E-07	2.0

The saturation remanence was measured on frozen samples suspended on acid-washed monofilament, after exposure to a 0.8-T unidirectional magnetic pulse. Conversion from magnetization to parts-per-billion equivalent was made using the saturation remanent magnetization (one-half of the saturation magnetization for magnetite, 4.8×10^5 A/m) and the specific gravity, 5.1 g/cm^3.

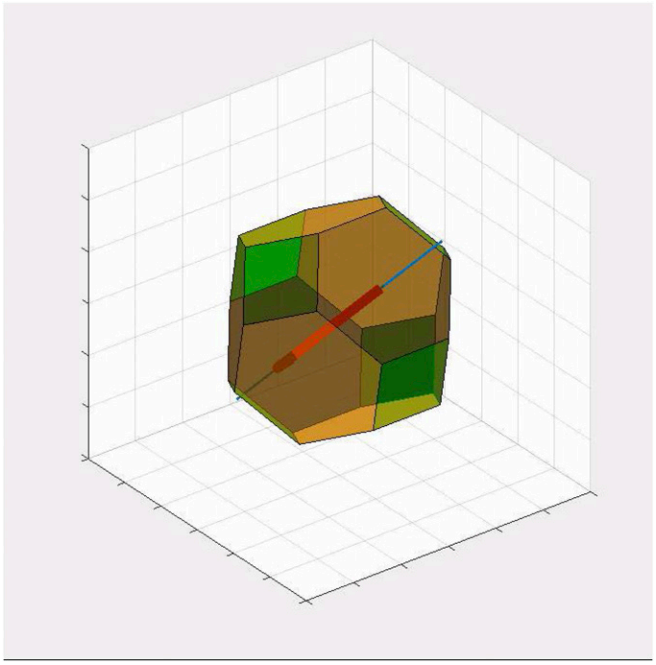

Movie S1. Simulation of a rotating magnetite nanocrystal. This movie shows a model of a typical magnetite crystal with a truncated octahedral morphology as it follows the precessing magnetic field in the experimental setup. Note that, by setting the angle of the rotating magnetic field to 45° from vertical, no point on the crystal surface is stationary with respect to the surrounding space (which is liquid water in reality). Brownian motion is not shown.

Movie S1